Design and modeling of the off-axis parabolic deformable mirror laboratory

Hari B. Subedi[a], Roser Juanola-Parramon [a,b], and Tyler D. Groff[a]

[a]NASA Goddard Space Flight Center, Greenbelt MD, 20771
[b] UMBC, MD

ABSTRACT

Coronagraph-equipped direct imaging missions need an active wavefront control system to cancel out the optical aberrations that degrade the performance of the coronagraphs. A fast steering mirror is used to control Line-of-Sight (LoS) pointing error caused by the telescope jitter. In addition to controlling other low-order aberrations such as astigmatism and coma, high stroke, high actuator density deformable mirrors (DMs) are also used to control the electric field at the required high spatial frequencies. We are designing a testbed to verify a different deformable architecture, where the powered optic in the optical train are controllable and have lower actuator count compared to the existing DMs with flat nominal surfaces. This simplifies the packaging issue for space missions and reduces both cost and risk of having the entire coronagraph instrument's performance depending on one or two high-actuator count DMs. The testbed would also be capable of testing different low-order wavefront sensing algorithms, which focuses in the near-term on a new adaptive Kalman filtering and gradient decent method to estimate the harmonic LoS errors that affect space telescopes. In the long run, we would test different machine learning techniques to estimate low-order aberrations and non-linear algorithms for digging the region of high contrast called the dark holes (DH).

1. INTRODUCTION

To achieve the high level of contrast required to directly image exoplanets, coronagraphic instruments must have active wavefront control system to estimate and compensate for aberrations of different temporal and spectral frequencies. The low-order wavefront sensor (LOWFS) estimates the dynamic aberrations such as line-of-sight (LoS) pointing errror and low-order aberrations such as focus, coma, sphere, and astigmatism. Algorithms such as speckle nulling,[2] electric field conjugation (EFC),[4] and stroke minimization[11] are used to calculate DM actuation to control quasi-static higher spatial frequency aberrations and dig the dark holes. The LoS pointing error is compensated by a tip/tilt mirror and a DM to cancel out the low-order aberrations. Conventionally, the dark hole digging techniques use two high actuator count flat DMs in the optical path, which results in any space mission having risk of single point failure. In addition to this risk, the minimum distance required between the DMs to effectively dig the dark holes for missions such as LUVOIR are so long that it causes packaging issues with the existing rocket fairings. Groff et al.[5] showed that the parabolic mirrors used in the optical train could be made deformable with fewer actuator counts than the flat DMs to reduce the risk of a space-based coronagraphic instrument by building redundancy into the DM control. This would also increase through put by reducing the number of optical surfaces. By placing the control surfaces on the sources of aberrations themselves, it is possible to increase the control bandwith too. We are working with vendors to manufacture off-axis parabolic DMs and are building a lab to experimentally verify the concept. The lab is designed to be a multipurpose lab to experimentally verify different low and high-order wavefront control algorithms.

We will start Section 2 by describing the wavefront control using parabolic DMs. Section 3 presents the planned layout of the lab. In Section 4, we will explain the different wavefront sensing and control algorithms that we intend to test in the lab. We begin this section (Section 4.1.2) by explaining the non-linear technique that minimizes the total energy in the dark hole. In Section 4.2, we will describe a new technique to estimate and control LoS pointing error that we would experimentally verify in the lab. This adaptive technique uses a

Further author information: (Send correspondence to Hari B. Subedi)
Email: hari.b.subedi@nasa.gov, Telephone: +13012865193

Kalman Filter (KF) and a gradient descent method to estimate the vibration induced LoS. In Section 4.3, we describe a machine learning LOWFS technique that we intend to verify in the lab and then we conclude the paper in Section 5.

2. WAVEFRONT CONTROL USING PARABOLIC DM

Groff et al.[5]used a shaped pupil coronagraph (SPC)[8] ripple3 design to do trade studies to determine the efficacy of using parabolic DMs for wavefront control. The study shows that 1) the full width half max (FWHM) of the actuator has a significant effect on the achieveable contrast and 2) the minimum number of the parabolic DM actuators required to achieve the desired high contrasts in broadband light is actually quite modest as long as there is one high actuator density DM at the pupil. Building on the results of this study, we did further simulations to find the limits of using parabolic DMs to do wavefront control. For the simulations presented in this section, we used the same SPC design but increased the size of the dark hole from $5-7.5\lambda/D$ to $5-12\lambda/D$. As we aim to determine the limits of the control achieved by the new DM architecture, we assume a perfect estimate of the wavefront and consider noiseless scenarios only. For the optimal DM command calculations, we use the EFC technique. We use the setup shown in Fig. 4 with a 32×32 Boston Micromachines DM at the pupil acess plane and two parabolic DMs - one as a focusing element and another as a collimating element as shown in the figure. The BMC DMs have a FWHM of 1.28 actuator and for the parabolic DMs we assume similar specifications like the ALPAO DM-97 which has the FWHM of 1.4 actuator.

First we determine the number of actuators required to dig a high contrast two symmetric dark holes at 20% bandwidth with the central frequency of 635nm. We introduce phase and amplitude aberrations at the pupil plane and phase aberrations at the OAP surfaces. Due to these aberrations, the mean contrast in the dark holes degrades to 1.2e-6(Fig. 2a). For this test, we use two parabolic DMs with 14x14, 16x16, and 18x18 actuators and the pupil access DM. From Fig. 2 a) it can be seen that using two 16x16 parabolic DMs improves the final contrast by more than an order of magnitude, but increasing the number of actuator to 18x18 does not have any significant improvement in the final contrast. We now test the improvement in the controllable bandwidth due to the parabolic DMs. For this test, we use same phase and amplitude aberrations as the actuator tests but change the bandwidth from 20% to 35% with an increment of 5%. For this test, we use two 16x16 parabolic DMs and a 32x32 BMC DM. The result of this test is presented in Fig. 2b) and Table 1.

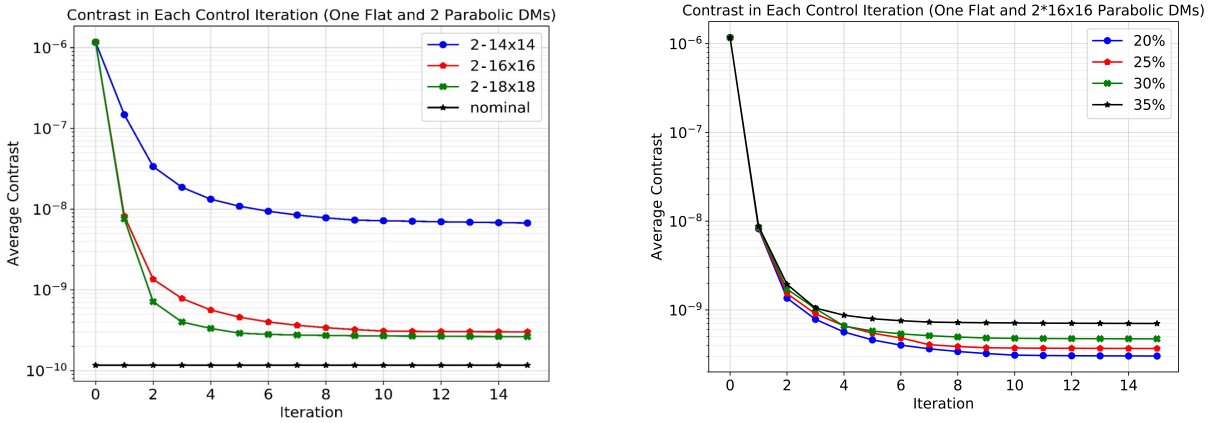

(a) Contrast vs iteration for different actuator count parabolic DMs.

(b) Contrast vs iteration for different bandwidths.

Figure 1: Contrast curves

Table 1: Final contrast for different bandwidths using two 16x16 parabolic DMs and one flat 32x32 pupil DM.

Bandwidth	Final Contrast
20%	3.1e-10
25%	3.9e-10
30%	4.7e-10
35%	7.1e-10

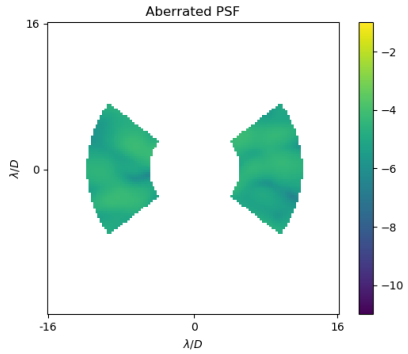

(a) Aberrated PSF due to phase and amplitude errors.

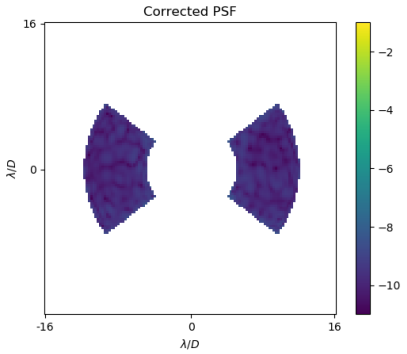

(b) Corrected PSF.

Figure 2: PSF before and after wavefront control using a pupil DM and two 16x16 parabolic DMs. The simulations use 20% bandwidth light centered at 635nm.

3. LAB LAYOUT

The layout of the proposed lab is shown in Fig. 4. A laser source will be used as a starlight emulator and collimated using an off-axis parabola (OAP) manufactured by Space Optics Research Lab (SORL). We will place a Physic-Instruments (PI) tip-tilt stage with a 2 inch flat mounted on it at the first pupil. The focusing OAP after the tip-tilt mirror will be a deformable mirror OAP. Using mutiple SORL OAPs of different focal lengths, multiple pupil access planes would be created. The Boston Micromachine (BMC) 32×32 - actuator DM will be placed at the next pupil plane. Subsequent pupil planes will have an apodizer and if required, a Lyot stop. At the coronagraphic focal plan,e we will have a Zernike phase mask. This mask will direct the rejected starlight to LOWFS camera and the remaining light to the science camera. Details of these optical elements are presented in the following section.

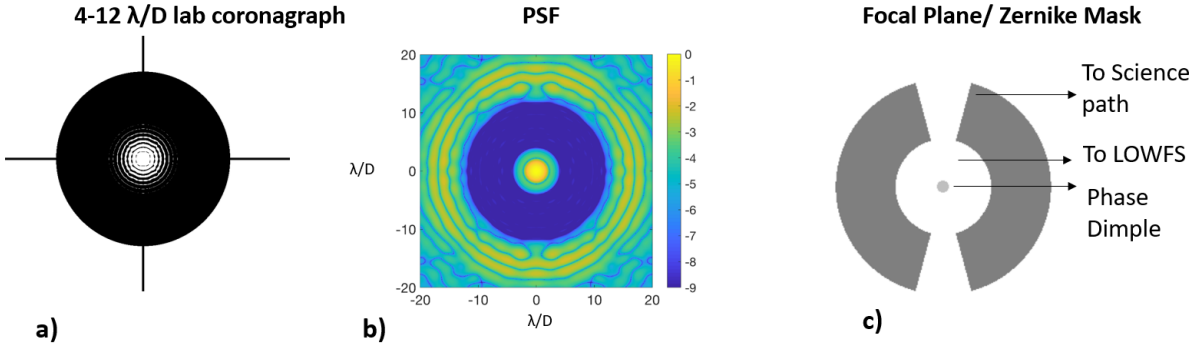

Figure 3: Optical masks to be used in the lab. a) Apodizer, b) point spread function (PSF) of the apodizer, c) focal plane mask (FPM).

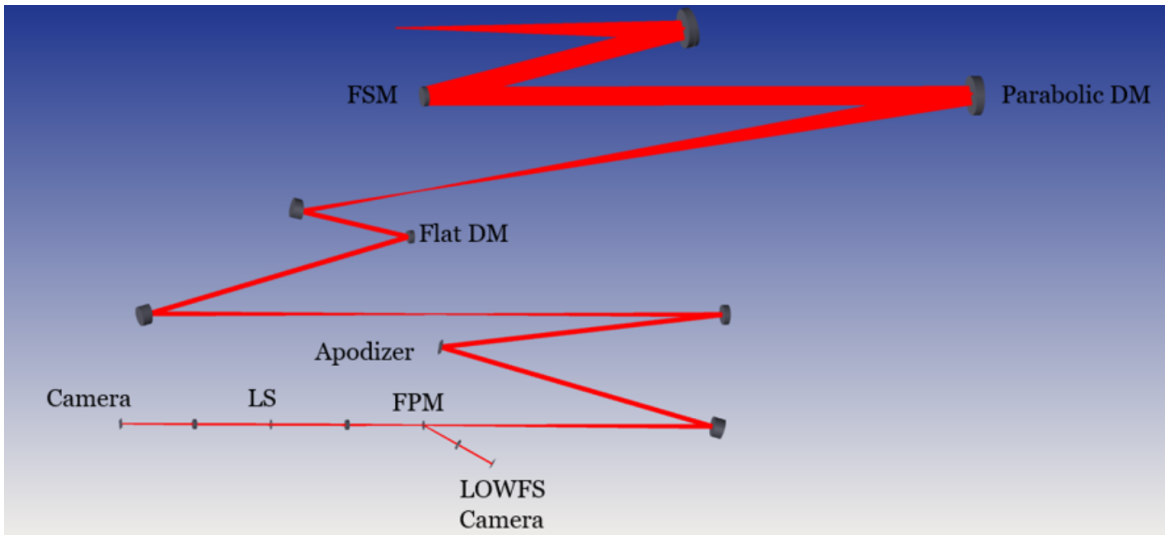

Figure 4: Layout of the Off-axis Parabolic Deformable Lab. Multiple pupil access planes are created using relay optics. A fast steering mirror (FSM), a 32×32 Boston Micromachines DM, an apodizer, and a Lyot stop (if required) will be placed in mutiple pupil planes. The coronagraphic focal plane will have a Zernike Phase Mask to direct the ligh to the LOWFS camera.

3.1 Apodizer

The apodizer shown in Fig. 3a) is a hard edge binary mask with the point spread function (PSF) as shown in Fig. 3b). The coronagraph has the average contrast of 1e-9 over the dark zone (DZ) of $4\lambda/D - 12\lambda/D$, where λ is the wavelength and D is the diameter. The apodizer is being manufactured using a carbon nanotube technology at NASA Goddard Space Flight Center.

3.2 Focal Plane Mask/ Zernike Phase Mask

The FPM has three different regions. The reflective central phase disk of the FPM (Fig. 3 c) has a diameter of $1.6\lambda/D$, a reflective region outside the phase disk that has a radius of $4.5\lambda/D$ and the outer bow-tie shaped transparent region from $4.5\lambda/D$ - $11.5\lambda/D$ at 150^o that lets light to the science path. The light that passes through the phase disk of the ZPM acts as a reference wavefront and interferes with the light passing outside the phase disk which contains the information on wavefront aberrations. The interfered light is then relayed to another pupil plane, where the detector records the intensity pattern. This intensity pattern is related to the phase variation of the telescope pupil plane and depends on the size of the phase mask and the phase change introduced by this mask. Using the intensity pattern at the detector plane and the least-squares-fit algorithm, the low-order abberations are inferred. This low-order wavefront sensor is called Zernike wavefront sensor.[1,3,9,10,12,14]

3.3 Parabolic Deformable Mirror

We are working with ALPAO to manufacture two off-axis parabolic DMs to meet the following minimum specifications:

- Pitch: 2.5 mm
- Actuators : 16x16 (functional)
- Effective Focal length: 1524mm
- Offset distance from the center: 254mm
- Resonant frequency: 500Hz

- Minimum frequency at phase lag of 45^o: 300Hz
- Maximum settling time (at +/-10%): 2ms
- Hysteresis: <10%
- Operating temperature: 25^o+/-5^oC
- Functional temperature: -5^oC to 45^oC
- OAP Shape accuracy < 30nm rms.

4. ALGORITHMS TO BE TESTED IN THE LAB

The following algorithms will be tested in the lab:

4.1 NonLinear Dark Hole Digging and Deformable Mirror Apodization

The goal of wavefront sensing and control is to dig the dark holes to the required contrast level in the presence of phase and amplitude abrrations. Techniques such as the EFC use the linear effects of the DM phase to achieve this goal. Non-Linear Dark Hole (NLDH) methods[6] have been proposed to minimize the starlight intensity in a given focal-plane area using an exact, non-linear, coronagraphic imaging model. This technique could be thought of as beam shaping with apodization. In this section, we will define the non-linear optimization problem and present the simulations results. The optimization problem can be stated as:

$$\underset{\mathcal{V}}{\text{argmin}} : f(\mathcal{V}) = \sum_{DH} I(\mathcal{V}, \phi_{abb}, A_{abb}), \tag{1}$$

where $\mathcal{V}$ is the DM voltage command and I is the intensity in the camera plane, which is a function of $\mathcal{V}$, phase error ϕ_{abb}, and the amplitude error A_{abb}. As $I_{DH} = |A_{DH}e^{\phi_{DH}}|^2$, the minimization problem is in fact minimizing the amplitude in the dark hole. To verify this algorithm in simulation, we considered three different coronagraphs - the SPC ripple 3, the $4 - 12\lambda/D$ lab coronagraph and the LUVOIR-B APLC coronagraph.

The setup for the simulation has a flat DM in a pupil plane, an apodizer in another pupil plane, a focal plane mask at the coronagraphic focal plane, a Lyot stop for the APLC, and a detector to take the final image. The cost function is simulated by forward propagating the DM phase (function of the independent variable $\mathcal{V}$ through the system and adding the estimates of the abberations. For this work, we assume perfect estimates and no noise. In future we would include noise model and real estimated values. For each forward step, we calculate the gradient using algorithmic differentiation[7] and supply the cost and the gradient to the python L-BFGS-B optimizer. In this section, we will present the simulation results of non-linear dark hole digging algorithm for different coronagraphs.

4.1.1 Monochromatic Simulation Results

First we will present the mononchromatic results for different setup and then present broadband results for the SPC ripple 3. For the monochromatic simulations, we have both phase and amplitude aberrations. For the broadband simulation, we modify the problem such that we dig a bigger dark hole at 20% broadband light from the existing nominal design. For the SPC (Fig. 5) coronagraph, we could dig a dark hole from starting degraded mean DH contrast of 1.1e-04 to 1.3e-10, 1.8e-05 to 7.1e-10 for the lab coronagraph (Fig. 6) and 1.4e-06 to 7.3e-11 for the LUVOIR-B coronagraph (Fig. 7).

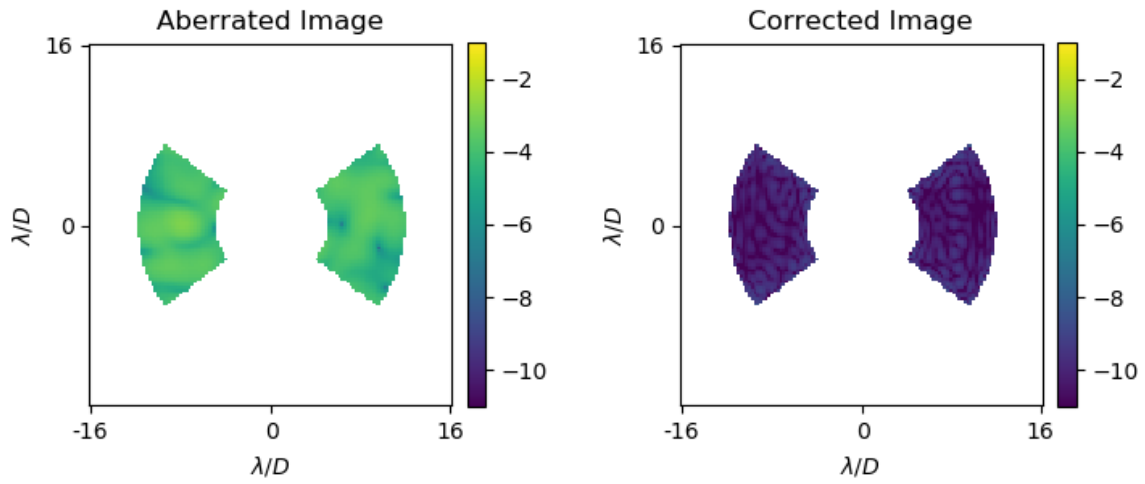

Figure 5: Dark hole digging with non-linear optimization for SPC. Aberrated PSF (left) with mean dark hole contrast of 1.1e-04 and (right) corrected PSF with mean contrast of 1.3e-10.

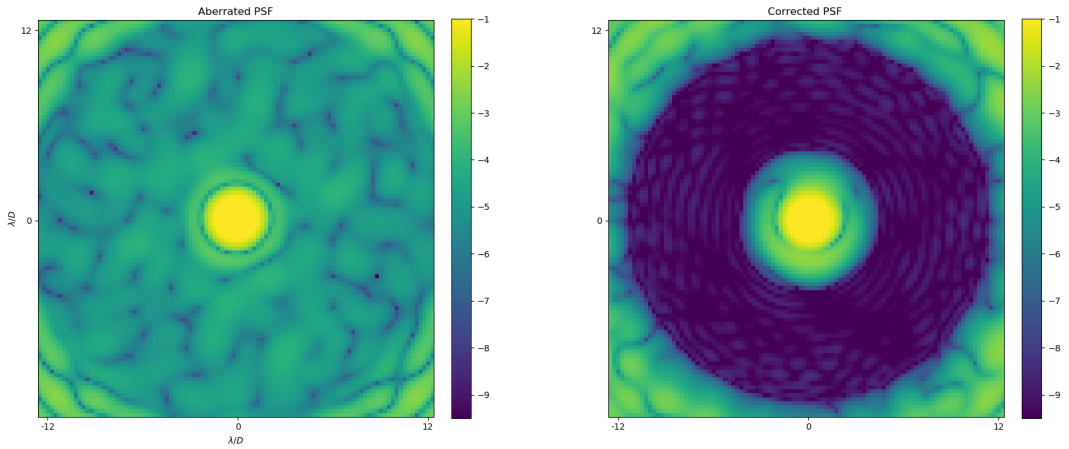

Figure 6: Dark hole digging with non-linear optimization for the lab coronagraph. Aberrated PSF (left) with mean dark hole contrast of 1.8e-05 and (right) corrected PSF with mean contrast of 7.1e-10.

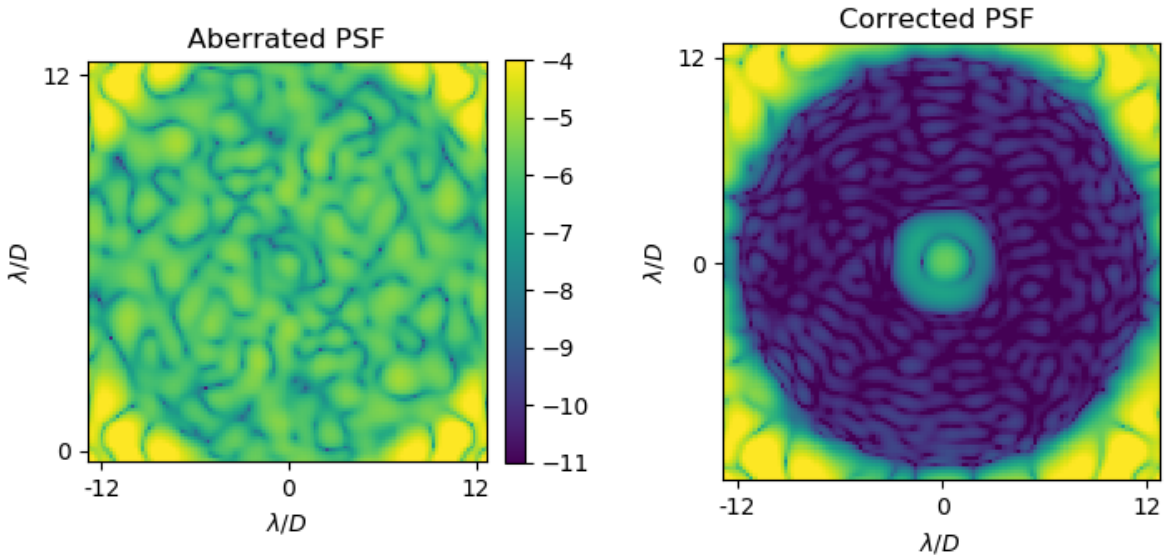

Figure 7: Dark hole digging with non-linear optimization for LUVOIR - B APLC. Aberrated PSF (left) with mean dark hole contrast of 1.4e-06 and (right) corrected PSF with mean contrast of 7.e-11.

4.1.2 Broadband simulation for DM Apodization

After we have shown that one DM could be used to dig two-sided and an annular dark hole, we applied this technique to improve contrast of existing SPC design at 20% bandwidth. For this simulation, we used a 256x256 SPC ripple3 design with nominal DH contrast of 6.5e-10 and used a 32x32 BMC DM to dig deeper dark holes with IWA of $5\lambda/D$ and OWA of $12\lambda/D$ with central frequency of 635 nm. As shown in Fig. 8, we were able to improve the mean dark hole contrast by an order of magnitude with similar throughput as the nominal SPC binary mask. This DM apodization technique would be useful in improving existing coronagraph designs. Using this optimization technique, we are currently working on using two DMs with classical Lyot type coronagraph to remove dependency in complex and difficult to manufacture apodizer and phase masks.

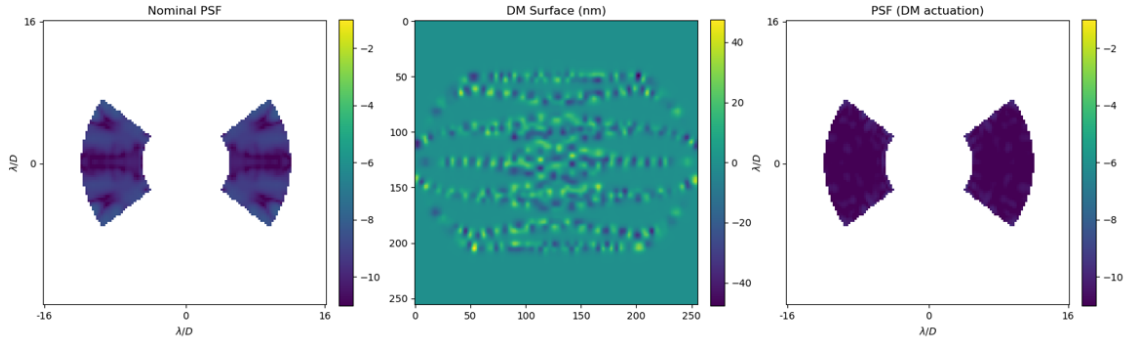

Figure 8: DM apodization with a SPC. The 256x256 SPC has average nominal DH contrast of 6.5e-10. Applying an optimal DM shape could improve the average DH contrast by more than an order of magnitude with only 2.5% reduction in throughput.

4.2 Adaptive Estimation for Line-of-Sight Jitter Estimate

The high frequency jitter caused by the reaction wheel (RW) of the telecopes are problematic for coronagrphic imaging. At each RW speed, the jitter contains frequency equal to the wheel speed and multiple harmonic frequencies. For the WFIRST, the RW speed changes form 10 Hz - 40 Hz over 18 hours and canceling a

fundamental frequency and a subharmonic would be sufficient. Most of the control scheme for controlling vibrational jitter assume a priori knowledge of the current wheel speed. In this testbed, we want to test a new adaptive technique[13] where we use the LOWFS camera measurement to determine the parameters of the system and the LoS jitter.

4.3 Low-order wavefront sensing using machine learning

We have used a single multilayer perceptron (MLP) to do phase retrieval and low-order sensing in simulations. A single MLP in essence solves for a linear relationship between the input and output. For the experiments, we will generate LOWFS images by introducing wide range of values for Zernike modes from Z_3 to Z_4. Then we will train the network using one set of LOWFS images and their corresponding Zernike coefficients. Once the network is trained, we will do LOWFS estimation using another set of data.

5. CONCLUSION

Wavefront control is essential for any coronagraph-equipped direct imaging missions. Multiple deformable mirrors are used for wavefront control to achieve the required contrast. In simulations, we show that making off-axis mirrors deformable achieves the goal of controlling wavefront. In doing so, we reduce the number of actuators required, thus reducing the cost and risk of failure. Using a 32x32 flat DM and two 16x16 parabolic DMs, we could achieve the high contrast and increase the control bandwidth. We are designing a lab to verify this new DM architeture and have provided required specifications to ALPAO to manufacture them. In this lab, we will also verify non-linear dark hole digging algorithm which minimizes the energy in the dark hole. We also intend to implement new line-of-sight jitter estimation and control technique which uses a kalman filter and a gradient descent. In addition to estimating LoS error, we intend to estimate other low-order modes such as focus, coma, and astigmatism using multilayer perceptron of artificial neural network.

6. ACKNOWLEDGEMENT

We would like to thank A.J. Riggs from JPL with the masks design and John Hagopian from the Nanoparticle consulting with the manufature of masks. The project is supported by NASA Goddard internal research and development (IRAD) and NASA HQ directed ExoSpec workpackage.

REFERENCES

[1] E. E. Bloemhof and J. K. Wallace. Phase contrast techniques for wavefront sensing and calibration in adaptive optics. In R. K. Tyson and M. Lloyd-Hart, editors, *Astronomical Adaptive Optics Systems and Applications*, volume 5169 of *Society of Photo-Optical Instrumentation Engineers (SPIE) Conference Series*, pages 309–320, December 2003.

[2] P. J. Bordé and W. A. Traub. High-Contrast Imaging from Space: Speckle Nulling in a Low-Aberration Regime. *APJ*, 638:488–498, February 2006.

[3] R. H. Dicke. Phase-contrast detection of telescope seeing errors and their correction. *APJ*, 198:605–615, June 1975.

[4] A. Give'on, B. Kern, S. Shaklan, D. C. Moody, and L. Pueyo. Broadband wavefront correction algorithm for high-contrast imaging systems. In *Society of Photo-Optical Instrumentation Engineers (SPIE) Conference Series*, volume 6691 of *Society of Photo-Optical Instrumentation Engineers (SPIE) Conference Series*, September 2007.

[5] T.D. Groff, A. Lemmer, and A.J. Riggs. A new deformable mirror architecture for coronagraphic instrumentation, 2016.

[6] O. Herscovici-Schiller, L. Mugnier, P. Baudoz, and et al. Towards the experimental validation of the non-linear dark hole on the thd bench, 2018.

[7] A. Jurling and J. Fienup. Applications of algorithmic differentiation to phase retrieval algorithms. *J. Opt. Soc. Am. A*, 31(7):1348–1359, Jul 2014.

[8] N. J. Kasdin, R. J. Vanderbei, D. N. Spergel, and M. G. Littman. Extrasolar Planet Finding via Optimal Apodized-Pupil and Shaped-Pupil Coronagraphs. *APJ*, 582:1147–1161, January 2003.

[9] M. N'Diaye, K. Dohlen, T. Fusco, and B. Paul. Calibration of quasi-static aberrations in exoplanet direct-imaging instruments with a Zernike phase-mask sensor. *AAP*, 555:A94, July 2013.

[10] Mamadou N'Diaye and et al. Dohlen. Design optimization and lab demonstration of zelda: a zernike sensor for near-coronagraph quasi-static measurements. volume 9148, pages 91485H–91485H–11, 2014.

[11] L. Pueyo, J. Kay, N. J. Kasdin, T. Groff, M. Mc Elwain, A. Give'on, and R. Belikov. Optimal Dark Hole Generation via Two Deformable Mirrors with Stroke Minimization. *ArXiv e-prints*, November 2011.

[12] F. Shi, K. Balasubramanian, R. Hein, R. Lam, D. Moore, J. Moore, K. Patterson, I. Poberezhskiy, J. Shields, E. Sidick, H. Tang, T. Truong, J. K. Wallace, X. Wang, and D. Wilson. Low-order wavefront sensing and control for WFIRST-AFTA coronagraph. *Journal of Astronomical Telescopes, Instruments, and Systems*, 2(1):011021, January 2016.

[13] H. Subedi, P. Varnai, and N. Kasdin. Adaptive estimation of line-of-sight jitter disturbance, 2017.

[14] J. Kent Wallace, Shanti Rao, Rebecca M. Jensen-Clem, and Gene Serabyn. Phase-shifting zernike interferometer wavefront sensor. volume 8126, pages 81260F–81260F–11, 2011.